Title
Impacts of longitudinal air velocity and fuel flow rate on flame radiative fraction in tunnel

Authors
Xu, Lin
Guo, Honghui
Ding, Chao
et al.

Publication Date
2020-10-01

DOI
10.1016/j.scs.2020.102336

Peer reviewed

Impacts of longitudinal air velocity and fuel flow rate on flame radiative fraction in tunnel

Lin Xu[1], Honghui Guo[2], Chao Ding[3,*], Yi Lu[1], Jinghan Liu[1]

1.Department of Thermal Engineering, Shandong Jianzhu University, Jinan, China, 250101

2.Tongyuan Design Group Co., Ltd., Jinan, China, 250101

3. Energy Technologies Area, Lawrence Berkeley National Laboratory, Berkeley, USA, 94720

* Corresponding author. Email address: chaoding@lbl.gov

ABSTRACT

Fires in tunnels have attracted special attention in recent years due to catastrophic fires, which cause huge human and economic losses. For accurate fire modelling and ventilation system design, it is critical to understand the correct radiative fraction (X_r) of the flame. Recent study has proved that X_r decreases with the increase of longitudinal air velocity in heptane pool fires. However, the impacts of longitudinal air velocity and fuel flow rate on X_r in propane or liquefied petroleum gas tunnel fires have not been studied. To fill the gap, this paper conducts two sets of fire experiments in a 1/20 reduced-scale wind tunnel using a porous burner. Unique visible flame shapes are observed and described by the 'back-to-back conical frustum'. The geometric parameters and their variations with the momentum flux ratio are discussed. In comparison with the experimental results, the radiation model using the proposed flame shape shows an 80% accuracy. The predictive radiative fractions of the two tests are calculated and compared with other tests from literature. The coupling effects of longitudinal air velocity and fuel flow rate on the flame radiative fraction are studied in detail. And their influences on key parameters of smoke extraction system are analyzed.

Keywords:

tunnel fire; radiative fraction; longitudinal air velocity; fuel flow rate; experiment

Nomenclature

A_f	Area of flame surface (m^2)	s	Offset distance of the visible flame (m)
C_T	Temperature correction factor (-)	v_{cri}	Critical velocity of longitudinal ventilation (m/s)
D_1	Diameter of the bottom surface of visible flame (m)	v_{in}	Longitudinal air velocity (m/s)
D_2	Diameter of the top surface of visible flame (m)	v_j	Fuel velocity at burner exit (m/s)
		X_r	Radiative fraction (-)
D_{max}	Maximum diameter of visible flame (m)	z	Height above the fire source (m)
D_s	Diameter of fire source (m)	ρ_j	Density of fuel (kg/m^3)
D_e	Hydraulic tunnel height (m)	ρ_{in}	Density of longitudinal airflow(kg/m^3)
E_f	Average emissive power at the flame surface (kW/m^2)	α	Flame tilt angle(degree)
		α_f	Tilt angle of flame axis (degree)
F	Geometric view factor (-)	η	Combustion efficiency (-)
G_j	Volume flow rate of fuel (l/h)	τ	Effective atmospheric transmissivity (-)
H	Flame length (m)	ΔH_c	Combustion heat of fuel (MJ/kg)
H_f	Length of flame axis (m)	ΔT_{max}	Maximum excess gas temperature beneath tunnel ceiling (K)
H_{ef}	Vertical distance above fire source		

	bottom (m)	Subscript	
J	Momentum flux ratio (-)	c	Convective
m_j	Mass flow rate of fuel(kg/s)	f	Flame
m_{flume}	Fire plume mass flow rate (kg/s)	j	Fuel
Q	Total heat release rate (kW)	hf	Heat flux meter or radiometer
Q_c	Convective heat release rate (kW)	in	Air flow
Q_r	Radiative heat release rate (kW)	p	Predicted theoretically
Q_c^*	Dimensionless heat release rate (-)	r	Radiative
q	Radiant heat flux (kW/m^2)		

1. Introduction

During the past decade, several tunnel fires with heavy casualties and property losses occurred in Europe: such as Mount Blanc (1999), Tauern (1999) and Gotthard (2001) (Lu, 2006, EBERL,2001). For example, 39 people were killed in the 1999 Mont Blanc Tunnel fire. The maximum heat release rate reached 300 MW and destroyed three quarters of a mile of the concrete dome. The repairs took three years to complete with a total loss of $200 million (Isolatek International,2020). After a series of severe fire accidents, fire safety in the tunnel attracts significant attentions and becomes a very important issue.

In the engineering design of ventilation and evacuation systems, the total heat release rate of fire(Q), especially its convective part (Q_c) is a key parameter. Its value directly affects the smoke flow rate (Li, Lei, & Ingason, 2011), smoke temperature (Tang, He, Chen, & Li, 2019; Yi, Wang, Yang, Wang, & Zhou, 2020) and critical velocity of longitudinal ventilation (Kennedy & Parsons, 1996) etc.

In order to facilitate the analysis and design, the radiative fraction (X_r) is introduced to characterize the radiation characteristics from the flame. Since the radiative heat is lost at the source, only the convective heat release rate (Q_c) transfers with the smoke flow in tunnel. Q_c can be calculated using X_r as follows:

$$Q_c = \left(1 - X_r\right)Q \tag{1}$$

To determine the value of Q_c, former studies mainly focused on understanding fire development and the influences of tunnel conditions on Q. The value of X_r is usually assumed to be a constant number, with a range of 0.2-0.4 (Yi, Wang, Yang, Wang, & Zhou, 2020; Ingason, Li, & Lönnermark, 2015; Mégret & Vauquelin, 2000; Liu, Yang, Xiao, Mao, & Yang, 2018). However, this assumption is based on oil pool fire data in the open still air (Koseki & Hayasaka, 1989; Markatos, Malin, & Cox, 1982). For tunnel fires, the follow questions still need to be explored: 1. Whether the values of X_r also vary with tunnel conditions, especially with different longitudinal air velocity? 2. As the air velocity changes, does X_r increase or decrease? 3.Whether X_r will further affect the design of the smoke exhaust system in the tunnel?

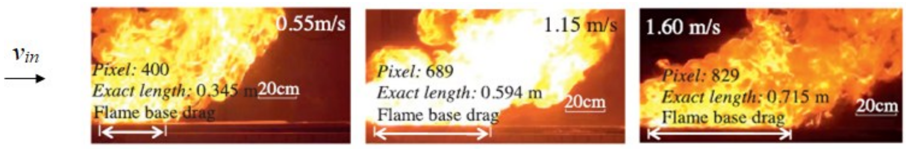

Fig.1 Flame images at different longitudinal air velocities for a 60cm heptane pool fire (Hu, L. et al.,2016)

As exhibited in Fig.1, the shape, volume and luminosity of the flame change significantly with the variation of the longitudinal air velocity (Hu, Zhang, Delichatsios, Wu, & Kuang, 2017). It demonstrates that, under the influence of the longitudinal air flow, X_r may depart from the usually assumed constant value of 0.2-0.4 (Turns, 2011; Delichatsios, & Orloff, 1989). This hypothesis has been recently proved by experiments (Zhang, Hu, Wu, Kostiuk, 2019). For the medium size square heptane and acetone pool fires, Zhang et al. found that X_r decreased with the increase of longitudinal air velocity. The decrease was observed to be more prominent as the pool size became smaller, and a bit more prominent for heptane than for acetone.

Besides the heptane pool fire, the porous burner using propane or liquefied petroleum gas (LPG) as fuel is often used as the fire source in the reduced scale tunnel experiments (Tang, He, Chen, & Li, 2019; Li, Lei, & Ingason, 2011). For this type of fire source, how to measure the flame radiative fraction in the reduced-scale tunnel experiments? How does the radiative fraction change with the longitudinal air velocity and fuel flow rate? How to evaluate their coupling effect on the value of X_r? These problems deserve further discussion.

The flame radiative fraction, X_r, can be calculated by:

$$X_r = \frac{Q_r}{Q} = \frac{Q_r}{m_j \eta \Delta H_c} \quad (2)$$

Where m_j and ΔH_c are the fuel mass flow rate and the heat of combustion, respectively. η is the combustion efficiency of the flame. For data presented by Johnson and Kostiuk (2000), the combustion efficiency of propane diffusion flame was found to be insensitive to crosswind, such that the lowest efficiency would be 99%. In the following analysis, the combustion efficiency of the flame is initially assumed to be 100%. Q_r is the total radiated energy, which cannot be easily measured and is usually inferred from the specific radiation prediction model.

The most widely used radiation prediction model is the single point source model (SPS). Sivathanu and Gore (1993) obtained X_r of jet diffusion flames of CH_4, C_2H_2, C_2H_4 in open still air. However, the distance between the radiometer and the flame center should be larger than 2.5D (D is the fire source diameter) to satisfy the point source assumption (Modak, 1977). In addition, the radiometer should be positioned at a vertical location equal to 50% of the flame height and perpendicular to the flame axis (Hamins, Klassen, Gore, & Kashiwagi, 1991). This seems to be somewhat more complicated and difficult to implement for the tilted flame in the longitudinal air flow. In Zhang's experiments, the radiometer was not perpendicular to the flame axis. To eliminate this position effect on the results, the horizontal distance between the pool and the radiometer was extended to 11.2~28D. Apparently, such a large distance is not practical in the reduced-scale tests, due to the rapid decrease of heat flux with the increasing distance (Guo, 2019).

To overcome the limitations of the SPS model, Hankinson and Lowesmith (2012) proposed the weighted multi-point source model (WMP) by assuming that the radiation emanated from a number of point sources distributed along the flame axis. Unlike SPS model, WMP model can provide good predictions in the near field of the fire source (Zhou, Zeng, Li, & Chaos, 2017). However, the accuracy of the WMP model is highly dependent on the determination of the weighting profile of the point sources, which needs a large number of measurement points. For example, the number of points was 50 in Zhou's analysis (2017). For a tilted flame, keeping the 50 radiometers perpendicular to the flame axis in the experiments is almost impossible. Namely, the WMP model is not suitable to study the influence of longitudinal airflow in the reduced-scale tunnel tests.

Because of the above limitations, other alternative methods should be introduced. The solid flame model may be a good option, which has been proved to accurately predict the incident radiant heat flux in near field of fire source (Mudan, 1987; Wan, Gao, Ji, Sun, Zhang, & Li, 2018). The model assumes that energy emission radiates uniformly over the entire visible flame envelope. The incident radiation flux, q_{hf}, received by the radiometer, is predicted as below:

$$q_{p,hf} = \tau_{hf} E_f F_{hf-A_f} \tag{3}$$

Where τ_{hf} is the effective atmospheric transmissivity between the radiometer and flame. In the near fire source region (path length less than 10m), τ_{hf}=1 (Wayne, 1991). $F_{hf\text{-}Af}$ is the geometric view factor from the radiometer to the flame, the detailed calculation method can be found in Guo's paper (2019). E_f is the average emissive power at flame surface, and can be calculated in the following manner:

$$E_f = \frac{m_j \Delta H_c X_r}{A_f} \tag{4}$$

Where A_f is the area of flame surface, m^2. Assuming that the measured radiant heat flux by the radiometer ($q_{m,hf}$) is equal to the predicted value ($q_{p,hf}$) from equation (3), substitution of the equations (2), (4) into equation (3) results in:

$$X_r = \frac{q_{m,hf} A_f}{m_j \Delta H_c F_{hf-A_f}} \tag{5}$$

According to equation (5), the most important step to determine X_r is to accurately describe the flame shape, and calculate A_f and $F_{hf\text{-}Af}$. As long as the incident radiant heat flux on the radiometer position by equation (3) can be well-predicted, this method can be used to determine the flame radiative fraction. As the radiometer's position is already considered and calculated by the geometric view factor, it does not matter whether the radiometer in the near area of fire source is perpendicular to the flame axis or not.

In conclusion, the flame radiative fraction is usually assumed to be a constant number, with an average of 0.3. However, this assumption is based on oil pool fire experiment data in the open still air, which may not be valid for fires in tunnel. Recent study has proved that X_r decreases with the increase of longitudinal air velocity in heptane pool fires. To fill the research gaps, this paper studies the impact of longitudinal air velocity and fuel flow rate on flame radiative fraction in propane or liquefied petroleum gas tunnel fires.

2. Experiments

2.1 Motivation of experiments

Therefore, a series of experiments are conducted in a 1/20 reduced scale model tunnel, including different combinations of fuel flow rate and longitudinal air velocity. Two gas burners with different sizes are chosen as the fire sources in the experiments. The geometric parameters of visible flame shape are described in detail. The incident radiative flux on the position of radiometer is predicted using theoretical calculation and compared with the experimental measurements. The values of X_r are further calculated, and its variations with the longitudinal air velocity and fuel flow rate are detailed analyzed.

2.2 Experimental rigs

As exhibited in Fig.2, the model tunnel corresponds to a 1/20 scale reduction of a standard two-lane road tunnel. It has 2 windows (0.5m*0.29m) made of transparent heat-resistant glass through which the flame can be observed. Fr scaling is used in the study and the scaling correlations of the model tunnel are presented in Table 1. Two porous burners are placed at the center, and align with the tunnel floor. A porous bed with a honeycomb on its top is located on a# for test 1. A 30mm diameter Bunsen burner (NG-2411BO0034, JUCHHEIM Inc.) is placed on b# for test 2, whose primary air is completely turned off during the experiments. The ventilation air is supplied through an 80mm steel pipe fitted with an orifice plate, providing a useful method to determine the volumetric flow. The longitudinal ventilation velocity is calculated by dividing the volumetric flow by the tunnel cross-sectional area. At different locations and aligned with the ground level, four water-cooled heat flux meters of type Schmidt-Bolter are placed to record the incident radiative flux. The incident radiant flux values are measured at 1#, 2# for test 1 and 3#, 4# for test 2, respectively. 20 measuring probes are set at the 1-1 section. The data are collected from the 20 sampling probes. A series of preprocessing are conducted, including condensing, drying, filtering, before the smoke are mixed to measure the mean concentrations of O_2, CO, CO_2. The schematic of the gas analysis system is also shown in Fig.2. The oxygen consumption calorimetry is used to determine the heat release rate in a tunnel fire. The experiments are conducted at different longitudinal air velocities (v_{in}) and at different fuel flow rates (G_j). The relevant data about the experimental cases and the chemical composition of LPG used in this paper are listed in Table 2 and Table 3.

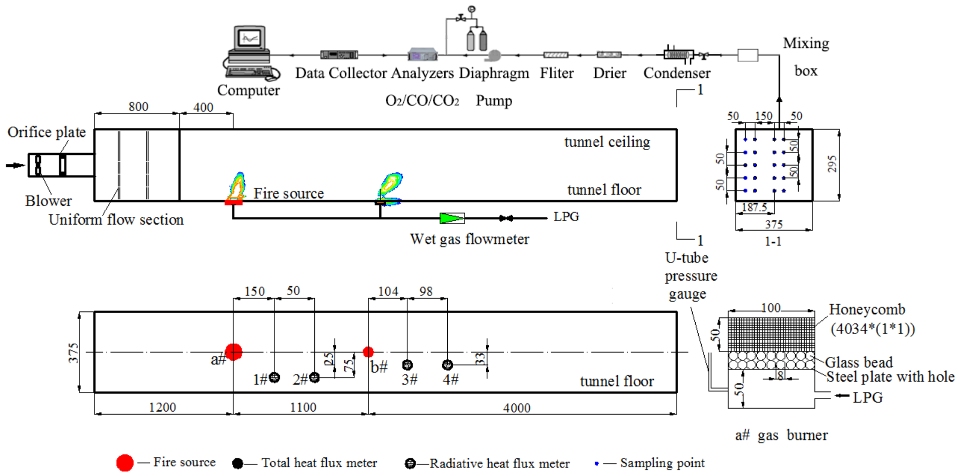

Fig.2. Schematic view of the experimental system (in mm).

Table 1

A list of scaling correlations for the model tunnel.

Length	Velocity	Flow rate	Heat release rate
1/20	$(1/20)^{1/2}$	$(1/20)^{5/2}$	$(1/20)^{5/2}$

Table 2

Relevant data of test cases used in this study.

Test	Fire source	D_s/cm	Q/kW	G_j /l/h	v_{in} /m/s	J[1]
test 1	*a#*	10	2.82~4.92	95~162	0.10~0.37	<0.03
test 2	*b#*	3	2.22~3.42	74~113	0.15~0.42	0.08-1.33

Note: 1. Momentum flux ratio $J=\rho_j v_j^2/\rho_{in} v_{in}^2$, where ρ_j and ρ_{in} is the density of fuel and air flow, kg/m^3. v_j is the fuel velocity at the burner outlet, m/s. According to the criterion identifying the flame configuration modes of jet in cross flow by Huang (1994), the flame behaviors for test 1 and test 2 are affiliated with down-wash and cross-flow dominated mode, respectively.

Table 3

Chemical composition of LPG used in the tests.

Fuel	Volume fraction	Fuel	Volume fraction	Fuel	Volume fraction	Fuel	Volume fraction
CH_4	2.88%	C_3H_6	0.01%	C_4H_8	0.38%	C_5H_{12}	0.67%
C_2H_6	0.06%	C_3H_8	1.44%	C_4H_{10}	94.55%	C_6H_{14}	0.01%

3. Results and discussion

3.1 Description of the flame shape

By use of a SONY camera (RX100), the visible flame videos are recorded and the visible flame shapes are distinguished using MATLAB software. And the mean flame shape (flame occurrence probability equals to 0.5 (Zukoski, Cetegen, &Kubota, 1985)), is introduced to describe the boundary of the visible flame to ignore the effect of the flame pulsation. Fig.3(a) and Fig.3(b) shows the sketches of the typical visible flames for test 1 and test 2. Some differences can be observed. In test 2, a region nearest to the fire source burns a blue flame and is almost invisible on the video records. By contrast, the blue flame zone of test 1 is negligible and the luminous yellow flame almost starts from the burner outlet. The reason may be due to different combustion efficiency and soot formation. Because of inadequate air supply and finer honeycomb aperture, for some experimental cases in test 1, large amounts of soot productions are observed in the experiments, as shown in Fig.3(a). Mudan (1987) and Johnson et al. (1994) have proved that thermal radiation from the blue flame region is small compared with that from the luminous yellow flame region. Therefore, the blue flame zone is not included in the flame shape model. Furthermore, as the upward velocity close to the fire source has relatively weak buoyancy compared to the longitudinal airflow, the visible flame is pushed and dragged towards the downwind direction.

To describe the visible flame shape, the tilted cylinder (Mudan,1987; Hankinson, & Lowesmith,2012; Palacios, Muñoz, Darbra, & Casal, 2012) and frustum of a cone (Kalghatgi, 1983; Johnson, Brightwell, & Carsley,1994) models were once used to successfully predict the radiant heat flux. Apparently, these two geometries are not appropriate for the test 1 and test 2. A 'back-to-back conical frustum' model is introduced in this paper to describe the visible flame shape, as shown in Fig.3(c). It can be described by one angle (α_f) and six lengths (H_f, H_{f1}, D_1, D_2, D_{max}, s). α_f is the angle between the axis of the conical frustum and the flame axis. D_1 and D_2 are the diameters of the conical frustum, and D_{max} is the maximum diameter of the flame. H_{f1} and H_f are the heights of the lower conical frustum and the entire back-to-back conical frustum, respectively. s is the offset distance deviating from the fire source. As mentioned above, due to the occlusion of the tunnel floor, the lower right corner (the part underneath the ground indicated by dotted lines) is eliminated from the 'back-to-back conical frustum' model.

As exhibited in Fig.3(d) and Fig.3(e), this newly proposed 'back-to-back conical frustum' agrees well with the visible flame envelopes for buoyant jet diffusion flame (Wang, Fang, Lin, Guan, & Wang, 2017) as well as for pool fire flame (Tang, Li, Zhu, Qiu, & Tao, 2015).

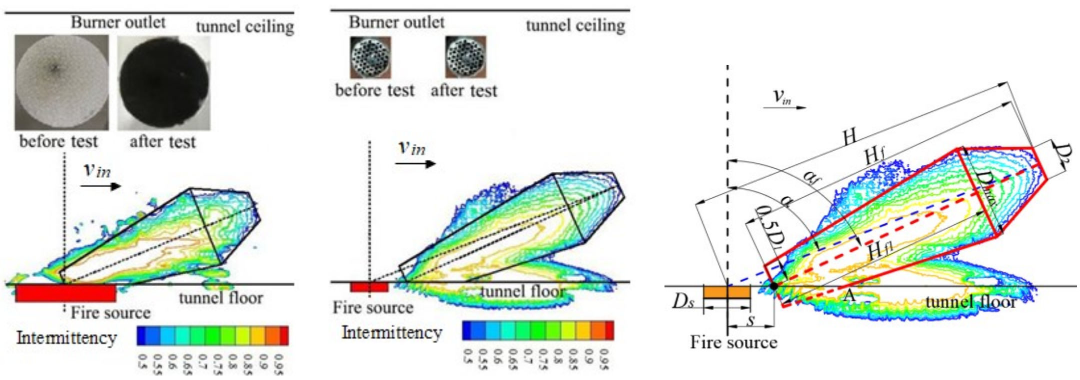

（a）Flame shape of test 1 (G_j=112.7 l/h, v_{in}=0.36m/s）

（b）Flame shape of test 2 (G_j=111l/h， v_{in}=0.37m/s）

(c) Geometric parameter definitions of a ‘back-to-back conical frustum’ model

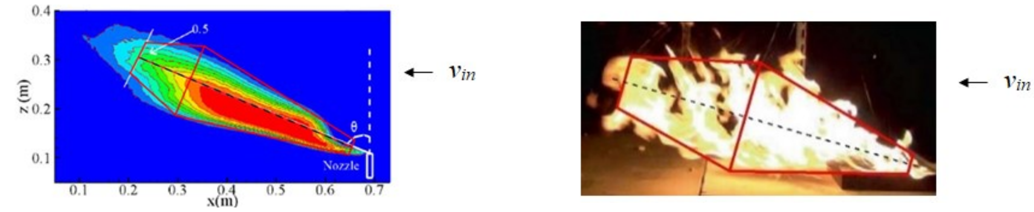

(d) Application example for a jet diffusion flame (Wang, Fang, Lin, Guan, & Wang, 2017)

(e) Application example for a pool fire flame (Tang, Li, Zhu, Qiu, & Tao, 2015)

Fig.3. Visible flame shapes of typical experimental cases, the geometric parameter definitions and application examples for a jet diffusion flame, a pool fire flame (elevation view).

3.2 Data processing method

Essentially, this kind of flame observed in the reduced-scale tunnel fire experiment is somewhat similar to the combusting gas jets issuing from the stack under a cross flow. Huang and Chang (1994) conducted experiments to study refinery flare stacks during emergency blow-offs in a chemical plant. The flame behavior and coherent structure of the combusting propane gas jet in a cross flow were analyzed. They employed the momentum flux ratio, defined by $J=\rho_j v_j^2/\rho_{in} v_{in}^2$, to identify different characteristic modes of flame configurations in the stability domain. Inspired by this data processing method, this paper firstly introduces and uses the momentum flux ratio J in tunnel fire parameter analysis. The following analysis examines the coupling effect of the longitudinal air velocity and the fuel flow rate on geometric parameters of the visible flame shape and radiative fraction.

3.3 Geometric parameters of the visible flame

(1) Flame diameter and flame trailing

As seen in Fig.4(a), the flame diameters are non-uniform along the flame axis for two tests, D_{max} is the much larger than D_1 and D_2. In comparison with fire source diameter (D_s), the clear expansion of flame diameter for test 2 is observed, D_{max}/D_s is about 2.5-4. For this reason, the ‘back-to-back conical frustum’ model is more suitable than the tilted cylinder model and the frustum of a cone model. The locations of maximum flame diameters are lower than $4/5H_f$, and decrease with the increasing J, as exhibited in Fig.4(b).

The phenomenon of flame trailing is evidently observed in the tests, which is common for liquid pool fires. As the density of butane gas (volume fraction>94% as shown in Table 3) is higher than that of air, it tends to remain at ground level, until it has been heated sufficiently to decrease its density below air density. Therefore, under the influence of longitudinal air flow, the visible flame is pushed and dragged towards the downwind direction. In this paper, the offset distance of the flame axis is used to characterize the flame trailing effect. As shown in Fig.4(c), the dimensionless offset distance (s/D_s) for test 2 is larger than that of test 1. For test 2, s/D is in the range of 0.5~1.6 and decreases with the increasing J. The horizontal offset effect of the flame axis is more evident for the experimental cases with a higher fuel flow rate.

(2) Length and tilt angle of flame axis

For the flame length (H), Majeski et al. (2004) suggested a simple linear correlation between the composite variable $H/\left(v_{in}\sqrt{c_f}\right)$ and $\sqrt{\rho_j v_j}D_s/v_{in}$ .Where c_f is the dilution of the fuel, for example c_f=1 for undiluted propane fuel.

As seen in Fig.4(d), the length of flame axis, H_f, also shows the similar linear correlation as following:

$$\frac{H_f}{v_{in}}=12.37\sqrt{\rho_j v_j}\frac{D_s}{v_{in}}+0.115 \quad (6)$$

The slope of equation (6) is smaller than those proposed by other experimental results. The difference may be due to the following reasons. Firstly, the values of H_f are smaller than H, as shown in Fig.3(c). Secondly, the criterion to determine the flame tip is different from each other. The flame tip is defined at 10% and 50% contours of flame occurrence probability by Majeski et al. (2004) and Lin (2015), respectively. The same criterion as Lin's (flame occurrence probability equals to 0.5) is used in this paper. The flame length defined by 10% contour of flame occurrence probability is larger than that by 50% contour of flame occurrence probability. So the slope of the Majeski's correlation is much larger. And the flame lengths by Pipkin and Sliepcevich (1964) are obtained by pure eye observation. The values are between Majeski's correlation and equation (6), as exhibited in Fig.4(d).

As seen in Fig.4(e), the tilt angles of flame axis show a decrease trend with the increasing J. The maximum α_f is no larger than 60 degrees for test 1 and test 2 cases. For test 2, the values of α_f are slightly less than Pipkin and Sliepcevich (1964)'s data and the correlation developed by Wang et.al (2017). It should be noted that Pipkin and Sliepcevich' data are based on the flame tilt angle (α), which is slightly larger than α_f, as shown in Fig.3(c). It can be easily imaged that the variation trend of α_f with J for test 2 is in good agreement with the Pipkin and Wang's experimental results.

As shown in Fig.4(e), there is large discrepancy between Wang's correlation and α_f values from test 1. The reason may be due to different jet outlet locations. In Wang's experiment, the tip of the nozzle is approximately 0.50 m above the floor of the tunnel, while the porous burner used in this paper is placed align with the tunnel floor. At low jet-to-wind momentum flux ratios as seen in Fig.3(d), the effects of entrainment and mixing of the fuel and air in the near wake region can no longer be ignored. Hence, flammable conditions can be established in both the near wake regions behind the nozzle and deflected jet. For this reason, the flame deflects through a large angle from the vertical axis of the nozzle. For test 1, the effect of mixing and combustion in the near wake regions behind the burner does not exist due to the obstruction of tunnel floor. And the values of α_f lower than that of Wang's correlation is reasonable.

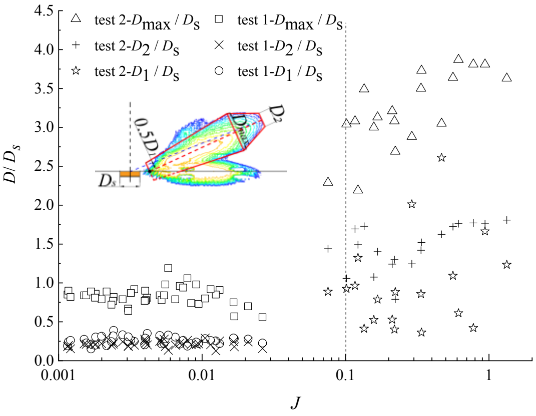

(a) Flame diameter

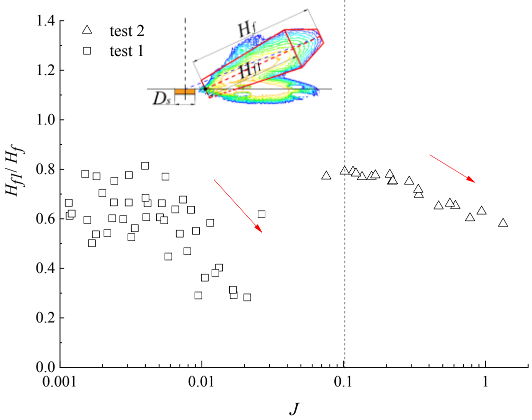

(b) Maximum flame diameter position

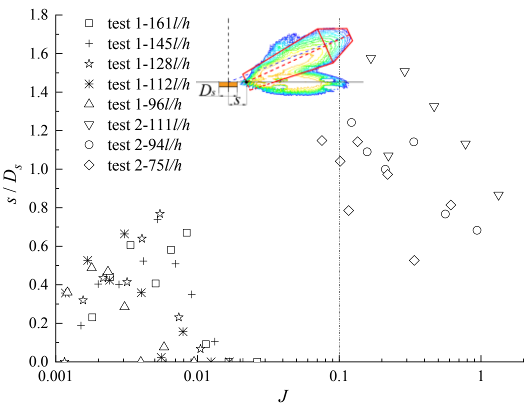

(c) Horizontal offset distance of flame axis

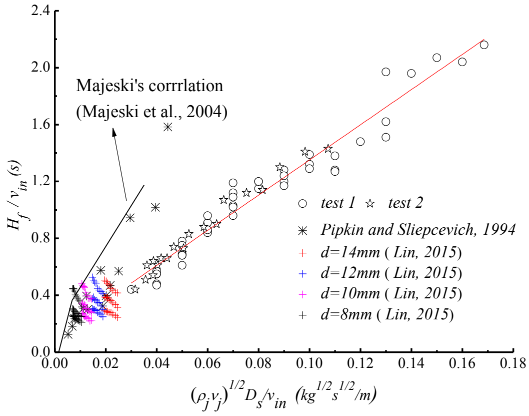

(d) Length of flame axis

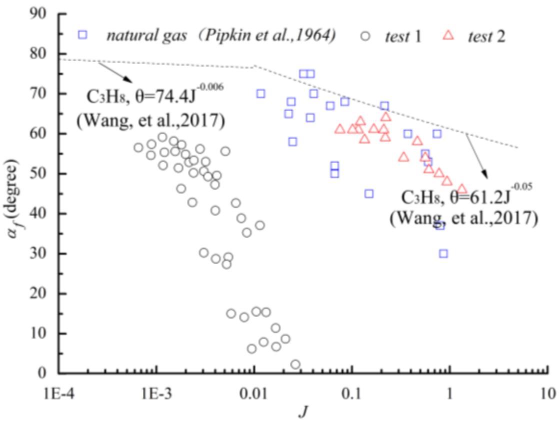

(e) Tilt angle of flame axis

Fig.4 Geometric parameters of the visible flames for test 1 and test 2

3.4 Experimental verification of radiation model

For test 1, the radiant heat flux at 1# on the ground ($q_{m,1\#}$) is measured, and its value is assumed to be equal to the predicted value ($q_{p,1\#}$) based on the 'back-to-back conical frustum' model. According to equation (3), the radiant heat flux at 2# ($q_{p,2\#}$) can be predicted as below:

$$q_{p,2\#} = q_{m,1\#} \frac{F_{2\#-A_f}}{F_{1\#-A_f}} \tag{7}$$

The geometric view factors from 1# and 2# to the flame can be calculated according to the method by Guo (2019). The calculation details will not be included in this paper.

Similarly, the measured radiant heat flux values at 2#, 3#, 4# are used as the reference. And the radiant heat flux values at other measuring points can be calculated and compared with the measured results, as shown in Fig.5. Apparently, the theoretical predictions of $q_{p,1\#}$, $q_{p,2\#}$, $q_{p,3\#}$, $q_{p,4\#}$ based on the 'back-to-back conical frustum' model agree well with the measurements. Most predicted heat fluxes are distributed within ±20% of the measured values. No predicted values are out of the range of 50%~150%. The above results show that the radiation model based on the 'back-to-back conical frustum' is accurate and can be used to predict the radiant heat flux and X_r.

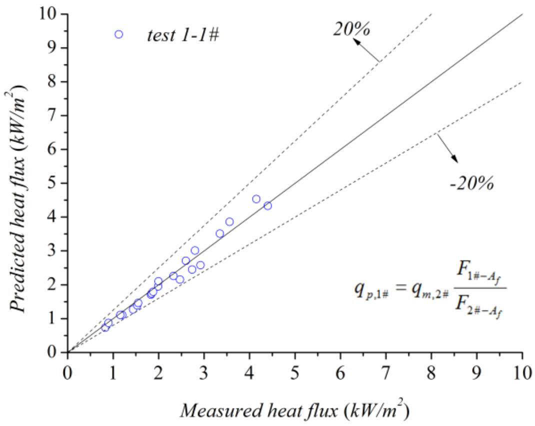

(a)Using 2# measurements as the reference（test 1）

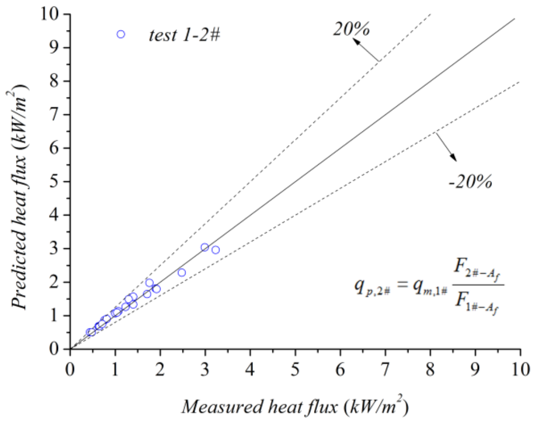

(b)Using 1# measurements as the reference（test 1）

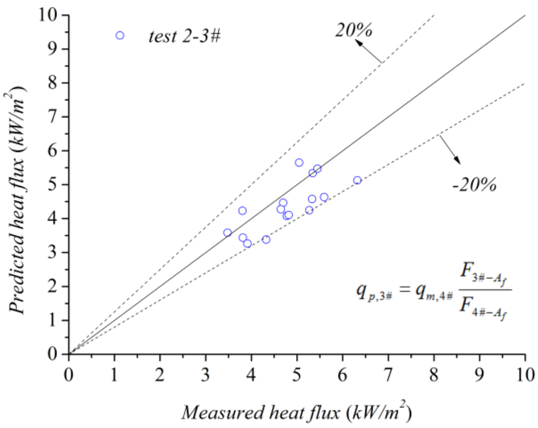

(c)Using 4# measurements as the reference（test 2）

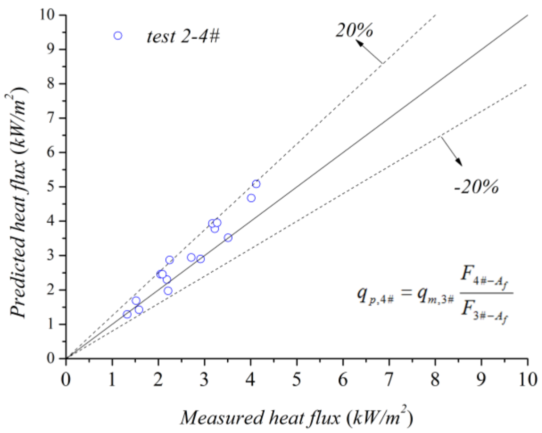

(d)Using 3# measurements as the reference（test 2）

Fig.5 Comparison of measured and calculated radiative heat flux of the measuring points. Note: the solid lines indicate equality of measured and predicted values.

3.5 Radiative fraction of flame

According to equation (5), the flame radiative fraction can be calculated and the values are shown in Fig.6 and Fig.7(a). Most of the experimental cases in test 1 and test 2 have two heat flux meters. For each measurement point, a radiative fraction is calculated. Their average value is taken as the final flame radiative fraction. For a small number of experimental cases of test 1, only one radiant heat flux (2#) is measured. Under this circumstance, the flame radiative fraction is calculated only based on 2# data. The error bar is also shown in Fig.6, It is observed that the calculated X_r based on different measurement points are consistent, which proves that the calculation method of radiation fraction is reliable and robust.

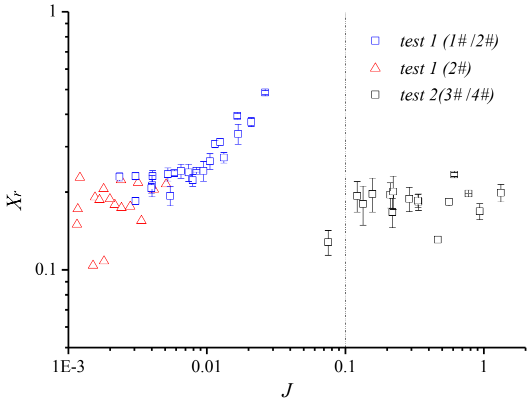

Fig.6 Relationship between radiative fraction and momentum flux ratio

3.6 Impact of X_r on tunnel ventilation and smoke extraction system

As exhibited in Fig.7(a), for the same fuel flow rate, the flame radiative fraction decreases with the increase of longitudinal air velocity. When the longitudinal air velocity increases in the same range, the value difference of X_r for the larger fuel flow rate is much higher than that of the smaller fuel flow rate.

Taking experimental cases (G_j=161l/h) as an example, as the air velocity increases from 0.1m/s to 0.36m/s, the values of X_r decrease from 0.45 to 0.1. According to equation (1), the convective heat rate of fire will increase from 0.55Q to 0.9Q. This means that some key parameters of tunnel ventilation and smoke extraction system will increase simultaneously, as shown in Table 4.

Table 4

Variations of some key parameters of tunnel smoke exhaust system with the changes of X_r.

Key parameters	Empirical formula[1]		Parameter variation[2]	Reference
Fire plume mass flow rate m_{plume} (kg/s)	$m_{plume} = 0.071\dfrac{Q_c^{1/3}}{z^{5/3}}$	$v' \le 0.19$	$m_{plume,2}/m_{plume,1} = 1.178$ $m_{plume,3}/m_{plume,1} = 1.083$ $m_{plume,3}/m_{plume,2} = 0.92$	Ingason et al. (2015)
Maximum excess gas temperature beneath tunnel ceiling ΔT_{max} (K)	$\Delta T_{\max} = 14.1 C_T \dfrac{Q_c^{2/3}}{H_{ef}^{5/3}}$	$v' \le 0.19$	$\Delta T_{\max,2}/\Delta T_{\max,1} = 1.389$ $\Delta T_{\max,3}/\Delta T_{\max,1} = 1.175$ $\Delta T_{\max,3}/\Delta T_{\max,2} = 0.846$	Ingason et al. (2015)
Critical velocity of longitudinal ventilation v_{cri} (m/s)	$\dfrac{v_{cri}}{\sqrt{gD_e}} = 0.4\left(\dfrac{Q_c^*}{0.2}\right)^{1/3}$	$Q_c^* \le 0.2$	$v_{cri,2}/v_{cri,1} = 1.178$ $v_{cri,3}/v_{cri,1} = 1.083$ $v_{cri,3}/v_{cri,2} = 0.92$	Wu et al. (2000)

Note: 1. Q_c=(1-X_r)Q, assuming a constant total heat release rate Q.

2. The subscript ‘1’, ‘2’ and ‘3’ correspond to the X_r=0.45, X_r=0.1 and X_r=0.3 case, respectively.

As mentioned above, the values of X_r in the former references are usually assumed to be 0.2~0.4, with a mean value of 0.3. Based on this value, the key parameters listed in Table 4 will underestimate by 8%-15.4% for the X_r=0.1 case, or overestimate by 8.3%-17.5% for the X_r=0.45 case.

Moreover, as exhibited in Fig. 7 (a), the influence of the fuel flow rate on the radiative fraction is presented in two ways: when v_{in}>0.22m/s, the radiative fraction is independent with the fuel flow rate; when v_{in}<0.12m/s, the radiation fraction increases significantly with the increase of the fuel flow rate. The potential cause of the higher X_r is the lower combustion efficiency.

According to the data by Johnson and Kostiuk (2000), the combustion efficiency of the flame in the above analysis is assumed to be 100%. In fact, the combustion efficiency may also be affected by the longitudinal air velocity and fuel flow rate. Some typical experimental cases for test 1 are chosen, and the total heat release rates of fire (Q) are measured according to the method of oxygen consumption calorimetry (Ingason, Li, & Lönnermark, 2015). In combination with the flow rate and combustion heat of fuel, the combustion efficiency of the flame is calculated further and shown in Fig.7(b). It should be noted that the sampling method of combustion gases used in this paper may lower the mean O_2, CO, CO_2 concentrations, due to the natural stratification in the direction of tunnel height at the 1-1 section. For this reason, the total heat release rate (Q) and combustion efficiency (η) are also underpredicted. But the difference of combustion efficiency with longitudinal air velocity cannot be ignored. And the variation trend of η with the increasing air velocity is opposite to X_r. This means that for the cases of low longitudinal air velocity, X_r may become larger.

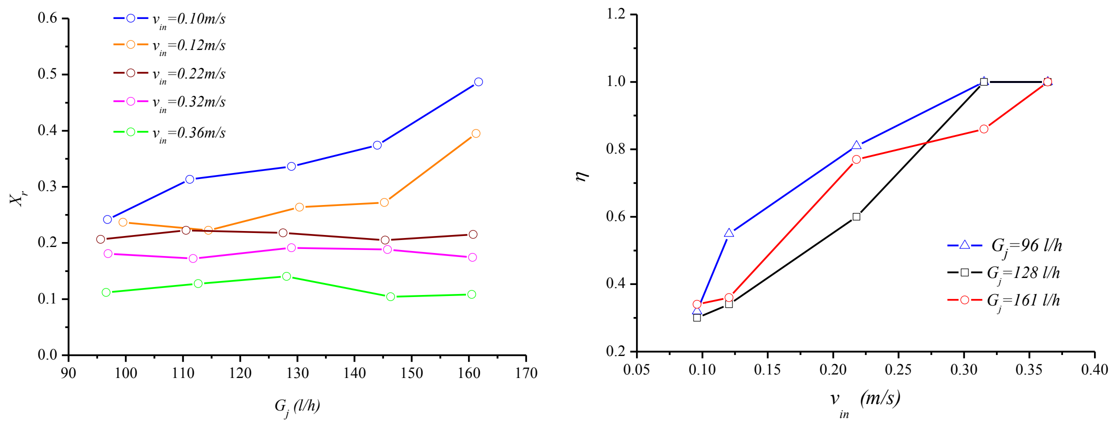

(a) X_r with v_{in} and G_j (b) Combustion efficiency with v_{in} and G_j

Fig.7 Radiative fraction and combustion efficiency against longitudinal air velocity and fuel flow rate of typical experimental cases (test 1)

3.7 Correlation of flame radiative fraction with composite variable

As exhibited in Fig.6, with the change of J, the values of X_r for test 1 are between 0.15 and 0.5, showing a positive correlation. For test 2, the values of X_r are between 0.15 and 0.25, the increase trend is not evident because of the high combustion efficiency and low soot formation.

To support engineering design, a regression equation is derived using our measurement data. Using equation (8) as follows, engineers can quickly estimate X_r values under different mass flow rate and ventilation velocity scenarios for ventilation and evacuation systems design.

$$\frac{X_r^{\frac{16}{11}} m_j^{\frac{4}{11}}}{v_{in}} = 14.497\left(\frac{\sqrt{m_j}}{v_{in}}\right)^2 - 0.7196\frac{\sqrt{m_j}}{v_{in}} + 0.0169 \qquad (8)$$

R^2=0.93

Where m_j is the mass flow rate of fuel, kg/s; v_{in} is the longitudinal air velocity, m/s. As shown in Fig.8, the above regression equation agrees well with the data by Brzustowski et al. (1975) and Lin (2015).

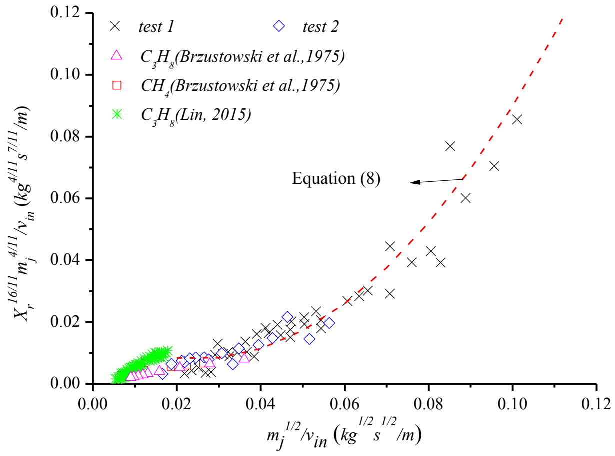

Fig.8 The regression equation of X_r , v_{in} and m_j.

4. Conclusions

In this paper, two sets of tunnel fire tests are conducted in a 1/20 reduced scale model tunnel. The flame videos are recorded and the incident radiative flux on tunnel floor are measured. Hereby, a theoretical model is proposed to predict the radiative fraction of tunnel fire. The main conclusions are:

(1) This paper introduces a novel 'back-to-back conical frustum' model to describe the visible flame shape of porous burner. In comparison with the experimental results, the radiation model using the proposed flame shape shows an 80% accuracy. It is used to predict the radiant heat flux of measuring points and to calculate the value of X_r.

(2) The momentum flux ratio J is used in this paper to examine the coupling effect of the longitudinal air velocity and the fuel flow rate. This data processing method has never been used in tunnel fire parameter analysis before in literature.

(3) The flame radiative fraction decreases with the increasing longitudinal air velocity. When v_{in} increased in the same range, the value difference of X_r for the larger fuel flow rate is much larger than that of the smaller fuel flow rate.

(4) For the cases of G_j=161 l/h, with the air velocity increasing from 0.1m/s to 0.36m/s, the values of X_r decrease from 0.45 to 0.1. Correspondingly, the fire plume mass flow rate, maximum excess gas temperature beneath tunnel ceiling and the critical velocity of longitudinal ventilation would increase by 17.8%, 38.9% and 17.8%, respectively.

(5) Large departure of X_r from the usually assumed constant value influenced the reliability of smoke extraction system. The key parameters listed in Table 4 are underpredicted for the case of X_r =0.1 by 8%-15.4%, or overpredicted for the case of X_r =0.45 by 8.3%-17.5%.

(6) The influence of the fuel flow rate on the radiative fraction is presented in two ways: when v_{in}>0.22m/s, the radiative fraction is independent with the fuel flow rate; when v_{in}<0.12m/s, the radiation fraction increases significantly with the increase of the fuel flow rate.

(7) A regression model is derived to support ventilation and evacuation systems design. Engineers can quickly estimate X_r values by considering the coupling impact of different mass flow rates and ventilation velocities.

Acknowledgement

The work was supported by the National Natural Science Foundation of China (grant numbers： No.51108254).

References

Brzustowski, T.A., Gollahalli, S.R., Gupta, M.P., Kaptein, M., & Sullivan, H.F. (1975). Radiant Heating from Flares, American Society of Mechanical Engineers, New York, 75-HT-4.

Delichatsios, M. A., & Orloff, L. (1989). Effects of turbulence on flame radiation from diffusion flames. Symposium on Combustion, 22(1), 1271-1279.

EBERL, G. (2001). The tauern tunnel incident. What happened and what has to be learned. International Transport Forum, 17-28.

Guo, H.H. (2019). Theoretical and experimental study on flame radiation near fire source in tunnel. A Thesis for the Master Degree, Shandong Jianzhu University, Jinan, China.

Hamins, A., Klassen, M., Gore, J., & Kashiwagi, T. (1991). Estimate of flame radiance via a single location measurement in liquid pool fires. Combustion and Flame, 86(3), 223-228.

Hankinson, G., & Lowesmith, B. J. (2012). A consideration of methods of determining the radiative characteristics of jet fires. Combustion and Flame, 159(3), 1165-1177.

Hu, L., Zhang, X., Delichatsios, M. A., Wu, L., & Kuang, C. (2017). Pool fire flame base drag behavior with cross flow in a sub-atmospheric pressure. Proceedings of the Combustion Institute, 36(2), 3105-3112.

Huang, R. F., & Chang, J. M. (1994). The stability and visualized flame and flow structures of a combusting jet in cross flow. Combustion and Flame, 98(3), 267-278.

Ingason, H., Li, Y.Z., & Lönnermark, A. (2015). Tunnel fire dynamics. First Edition, Spring Verlag, New York.

Isolatek International (2020). Tunnel Fires. Accessed 5 13, 2020. https://reppel.nl/storage/assets/isolatek-type-m-ii-tunnel-fires-engels.pdf.

Johnson, A.D., Brightwell, H.M., & Carsley, A.J. (1994). A model for predicting the thermal radiation hazards from large-scale horizontally released natural gas jet fires. I CHEME symposium series No.134,123-142.

Johnson, M. R., & Kostiuka, L. W. (2000). Efficiencies of low-momentum jet diffusion flames in crosswinds. Combustion and Flame, 123(1-2), 189-200.

Kalghatgi, G.T. (1983). The visible shape and size of a turbulent hydrocarbon jet diffusion flame in a cross-wind, Combust and Flame, 52, 91-106.

Kennedy W.D., Parsons B. (1996). Critical velocity: past, present and future. Seminar of smoke and critical velocity in tunnels, London, UK, 305-322.

Koseki, H., & Hayasaka, H. (1989). Estimation of thermal balance in heptane pool fire. Journal of Fire Sciences, 7(4), 237-250.

Li, Y. Z., Lei, B., & Ingason, H. (2011). The maximum temperature of buoyancy-driven smoke flow beneath the ceiling in tunnel fires. Fire Safety Journal, 46(4), 204-210.

Lin, S.B. (2015). Influence of Cross-wind on Low-momentum Turbulent Jet Diffusion Flame's Image Parameters and Combustion Characteristics. A Thesis for the Doctor Degree, State Key Laborary of Fire Science, University of Science and Technology of China, Hefei, China.

Liu, Y., Yang, D., Xiao, Y., Mao, S., & Yang, M. (2018). Combining diverse driving forces for smoke control in complex urban traffic link tunnels (utlts) using one-dimensional flow modelling. Sustainable Cities and Society, 43, 265-274.

Lu, Y. (2006). Mont Blanc Tunnel Fire. Labor Insurance (10), 66-69.

Majeski, A. J., Wilson, D. J., & Kostiuk, L. W. (2004). Predicting the length of low-momentum jet diffusion flames in crossflow. Combustion Science and Technology, 176(12), 2001-2025.

Markatos, N. C., Malin, M. R. & Cox, G. (1982). Mathematical modelling of buoyancy-induced smoke flow in enclosures. International Journal of Heat and Mass Transfer, 25(1), 63-75.

Mégret, O., & Vauquelin, O. (2000). A model to evaluate tunnel fire characteristics. Fire Safety Journal, 34(4), 393-401.

Modak, A. T. (1977). Thermal radiation from pool fires. Combustion and Flame, 29, 177-192.

Mudan, K. S. (1987). Geometric view factors for thermal radiation hazard assessment. Fire Safety Journal, 12(2), 89-96.

Palacios, A., Muñoz, M., Darbra, R. M., & Casal, J. (2012). Thermal radiation from vertical jet fires. Fire Safety Journal, 51, 93-101.

Pipkin, O.A., & Sliepcevich, C.M. (1964). Effect of wind on buoyant diffusion flames. Initial correlation. Industrial and Engineering Chemistry Fundamentals, 3,147-154.

Sivathanu, Y. R., & Gore, J. P. (1993). Total radiative heat loss in jet flames from single point radiative flux measurements. Combustion and Flame, 94(3), 265-270.

Tang, F., He, Q., Chen, L., & Li, P. (2019). Experimental study on maximum smoke temperature beneath the ceiling induced by carriage fire in a tunnel with ceiling smoke extraction. Sustainable Cities and Society, 44, 40-45.

Tang, F., Li, L. J., Zhu, K. J., Qiu, Z. W., & Tao, C. F. (2015). Experimental study and global correlation on burning rates and flame tilt characteristics of acetone pool fires under cross air flow. International Journal of Heat and Mass Transfer, 87, 369-375.

Turns, S. R. (2011). Turbulent nonpremixed flames. An Introduction to Combustion: Concept and Applications, McGraw-Hill Education, 486-525.

Wan, H., Gao, Z., Ji, J., Sun, J., Zhang, Y., & Li, K. (2018). Predicting heat fluxes received by horizontal targets from two buoyant turbulent diffusion flames of propane burning in still air. Combustion and Flame, 190, 260-269.

Wang, J. W., Fang, J., Lin, S. B., Guan, J. F., & Wang, J. J. (2017). Tilt angle of turbulent jet diffusion flame in crossflow and a global correlation with momentum flux ratio. Proceedings of the Combustion Institute, 36(2), 2979-2986.

Wayne, F. D. (1991). An economical formula for calculating atmospheric infrared transmissivities. Journal of Loss Prevention in the Process Industries, 4(2), 86-92.

Wu, Y., Bakar, M.Z.A., 2000. Control of smoke flow in tunnel fires using longitudinal ventilation systems- a study of the critical velocity. Fire Safety Journal, 35, 363-390.

Yi, L., Wang, X., Yang, Y., Wang, Y., & Zhou, Y. (2020). A simplified mathematical model for estimating gas temperature and velocity under natural smoke exhaust in sloping city tunnel fires. Sustainable Cities and Society, 55.

Zhang, X., Hu, L., Wu, L., & Kostiuk, L.W. (2019). Flame radiation emission from pool fires under the influence of cross airflow and ambient pressure. Combustion and Flame, 202, 243-251.

Zhou L., Zeng, D., Li, D., & Chaos, M. (2017). Total radiative heat loss and radiation distribution of liquid pool fire flames. Fire Safety Journal, 89, 16-21.

Zukoski, E.E., Cetegen, B.M., & Kubota, T. (1985). Visible structure of buoyant diffusion flames. Symposium (international) on Combustion, 20(1), 361-366.